Oil shale powders and their interactions with ciprofloxacin, ofloxacin, and oxytetracycline antibiotics

Asmae Gouza, Sanaa Saoiabi, Miloud El Karbane, Sylvie Masse, Guillaume Laurent, Ahmed Rami, Ahmed Saoiabi, Abdelaziz Laghzizil, Thibaud Coradin

Oil shale powders and their interactions with ciprofloxacin, ofloxacin and oxytetracycline antibiotics

Asmae Gouza[a], Sanaa Saoiabi[a], Miloud El Karbane[b], Sylvie Masse[c], Guillaume Laurent[c], Ahmed Rami[b], Ahmed Saoiabi[a], Abdelaziz Laghzizil[a,*], Thibaud Coradin[c,*]

[a] *Laboratoire de Chimie Physique Générale, Université Mohammed V, Faculté des Sciences BP.1014 Rabat, Morocco*

[b] *Laboratoire National de Contrôle des Médicaments, Rabat, Morocco*

[c] *Sorbonne Universités, UPMC Univ Paris 06, CNRS, Collège de France, UMR 7574, Laboratoire de Chimie de la Matière Condensée de Paris, F-75005 Paris, France*

[*]**Corresponding authors:**

T. Coradin, Laboratoire de Chimie de la Matière Condensée de Paris, Université Pierre et Marie Curie, 4 place Jussieu,, F-75005 Paris, France Tel:33-1-44-27-55-17, Fax: 33-1-44-27-47-69, Email address: thibaud.coradin@upmc.fr

A. Laghzizil, Laboratoire de Chimie Physique Générale, Université Mohamed V, Faculté des Sciences BP.1014 Rabat, Morocco, Email address: laghzizi@fsr.ac.ma

ABSTRACT

The interaction of oil shale, as a widespread sedimentary rock, with common antibiotics ofloxacine, oxytetracycline and ciprofloxacine was studied. The selected Moroccan deposit and its thermally-treated forms were fully characterized from a chemical and structural point of view, indicating the prevalence of quartz as a mineral component together with aluminium- and iron-rich phase that are converted into Al-doped iron oxide phases upon heating. The presence of 4 wt% organics was also detected, that was removed at 550°C without significant loss of specific surface area. The pseudo-second-order kinetic model and Langmuir equation were found the most adequate to reproduce the kinetics and isothermal sorption experiments. These analyses enlighten the contribution of the organic matter on antibiotics retention as well as the key role of hydrophobic interactions on the molecule-mineral surface interactions. Our results emphasize the possible contribution of raw oil shale in the accumulation of antibiotics in soils and suggest that thermally-treated oil shell powders can constitute cheap mineral sorbents for environmental cleaning.

Keywords: Oil shale; Antibiotics; Quartz; Retention; Solid state NMR; Mineral sorbents

Introduction

The term “oil shales” refers to mineral deposits widely applied in fuel and oil industrial process for unconventional oil production that converts kerogen into shale oil by pyrolysis, hydrogenation, or thermal dissolution (Aboulkas and El Harti 2009; Bruant et al. 2001). Over the last few years, they also have attracted a huge interest as gas reservoir (Holditch 2013; Ross and Bustin 2009). The composition of these rocks varies from one deposit to another but are primarily composed of the amorphous silica and quartz in association with a wide assortment of accessory minerals, mainly carbonates, clays, and metal oxides (Fernandes Machado and Miotto 2005; Wang et al. 2009). Oil shales can be classified according to their chemical composition including inorganic and organic matters. Much of the organic matter in oil shale is the main component for oil production and gas generation but the inorganic ions, including iron, aluminium and calcium also have a large impact on their properties (Bernard et al. 2010). Altogether, these chemical properties suggest that oil shale can have a strong affinity for both organic and inorganic species. This was demonstrated in several studies demonstrating the adsorption of harmful organic molecules (Al-Qodah 2000; Irha 2000; Zhu et al. 1988), including pesticides (Al-Qodah et al. 2007a; Tütem et al. 1998) and toxic metals (Shawabkeh et al. 2004) by oil shale. Efficient removal of reactive dyes by oil shale in continuous fixed bed conditions was also reported (Al-Qodah and Lafi 2003). However, most of these studies used oil shale ash (i.e. carbonized deposits) whereas very little is known about the properties of the raw oil shale minerals (Ichcho et al. 2005).

Here, we focused on the interactions of raw oil shale deposits with antibiotics whose increasing concentration in soils and domestic, agricultural and industrial wastewaters has become a major environmental concern (Kümmerer 2009a,b). We selected non-biodegradable quinolone antibiotics ofloxacin (OFL), oxytetracycline (OTC) and ciprofloxacin (CIP) that are among the more commonly used and have high persistence in the environment (Carasquillo et al. 2008; Golet et al. 2003; Kagle et al. 2009; Vasudevan et al. 2009). A detailed chemical and structural analysis was performed on the raw material as well as its thermally-treated forms. Their interaction with Moroccan oil shale powders was investigated via kinetics and sorption isotherms. These studies allow for an elucidation of the relative contribution of the organic matter and mineral phases on the antibiotic retention.

Materials and Methods

Chemicals

Ciprofloxacin (1-cyclopropyl-6-fluoro-4-oxo-7-piperazin-1-yl-quinoline-3-carboxylic acid, CIP), Ofloxacin ((R,S)-9-fluoro-2,3-dihydro-3-methyl-10-(4-methyl-1-piperazinyl)-7-oxo-7H-pyrido [1,2,3-de]-1, 4-benzoxazine-6-carboxylic acid, OFL) and Oxytetracycline ((2Z)-2-[amino(hydroxy)methylidene]-4-(dimethylamino)-5,6,10,11,12a-pentahydroxy-6-methyl-4,4a,5,5a-tétrahydrotetracene-1,3,12-trione, OTC) were purchased from Aldrich (**Fig. 1**). The values of the octanol-water partition coefficients XlogP3 were obtained from the PubChem (NCBI) database (http://pubchem.ncbi.nlm.nih.gov).

Sedimentary oil shale and thermal treatments

The OST oil shale used in this study comes from Tanger ores located in the north of Morocco, nearby to the strait of Gibraltar which connects the Mediterranean Sea with the Atlantic. Prior to use, this material requires treatments such as crushing and washing. The fraction of 100-500 µm grain size was washed with distilled water several times to remove the soluble matter. The chemical composition of the raw deposit OST 100 obtained from elemental analysis is 80 % SiO_2, 7.9 % Al_2O_3, 2.17 % Fe_2O_3, 1.21 % MgO, 0.84 % CaO, 0.64% K_2O, 0.31 % Na_2O, 0.2 % TiO_2, 0.14 % ZnO (Gouza et al. 2014). Its thermal degradation was studied by thermogravimetric analysis (TGA) under air at a $5°.min^{-1}$ heating rate

Characterization

The OST550 and OST950 powders were obtained by heating the raw powder for 3 hours under air at 550°C and 950°C, respectively. The samples were analyzed by X-ray diffraction (XRD) using a Bruker D8 Advance diffractometer opertaing with at monochromatic Cu Kα radiation. Their specific surface area S_{BET} was determined by performing N_2-sorption experiments at 77 K on a BELSORP-max instrument and applying the Brunauer- Emmett-Teller (BET) equation.

Solid state NMR studies were performed on a Bruker Avance III spectrometer operating at 300.29 MHz for ^1H and 59.66 MHz for ^{29}Si. 7 mm zirconia rotors were spun at 5 kHz using a broadband dual resonance ^1H-X Magic Angle Spinning (MAS) probe. For High Power DECoupling (HPDEC) experiments, a SPINAL64 $\{^1H\}$ decoupling was applied during acquisition (ν_{1H}=44 kHz). ^{29}Si HPDEC spectra were recorded using a 30° pulse, a recycle delay of 10 s that allows to get semi-quantitative information for all the species, 720 transients for the raw and the 550°C heat-treated sample, 1440 transients for the 950°C heat-treated sample. Such acquisition conditions allow getting the signal from all the species constitutive of the material, those coming from the amorphous parts of the material that will relax very quickly, as well as those coming from the most crystalline parts (here namely, quartz) that require longer relaxation delays. For the purpose of the spectral comparison, we normalized at 100% the intensity of the Q^4 signal of quartz at -107 ppm. For ^1H experiments, a recycle delay of 2

s was operated, that is respectful for T1 relaxation. For ^{27}Al 3Q-MAS NMR experiments, a 4 mm MQ-MAS probe was used and sample were spun at 14 kHz for MAS. The resonance frequency was 78.24 MHz for ^{27}Al, the recycle delays were 100 ms or 1 ms, supplemented by 5.1 ms for acquisition delay. This was done in order to discriminate the rapid relaxation species from the other ones, and pulses of 1.55 µs, 0.78 µs and 65 µs were used for excitation, conversion and z-filter, respectively. To obtain a good signal to noise ratio on the 2D maps, 57.600 transients were necessary for the 1 ms experiment and 14.400 transients for 100 ms one, for the raw material and the 950°C heat-treated sample as well. Spectra were sheared before Fourier Transform. Guidelines were added on the figures to indicate the CS (chemical shift) and QSI (Quadrupolar-Induced Shift) contributions.

Antibiotics retention experiments

The kinetics of antibiotics retention by oil shale powders were followed in batch experiments conducted at 25°C by adding 200 mg of sorbent to 100 mL of an aqueous solution containing 20 mg L^{-1} of antibiotics acidified to pH 5 except when noted. Sorption isotherm studies were conducted in the 0-150 mg L^{-1} antibiotic concentration range at the same pH. At selected time interval, the suspensions were sampled by centrifugation and the antibiotic concentration in supernatant was monitored using a UV-visible spectrophotometer (Perking Elmer Lamda II) at 354 nm, 273 nm and 295 nm for OTC, CIP and OFL. For low level of antibiotics, all UV-visible analyses were controlled by high performance liquid chromatography (HPLC) (Bouyarmane et al. 2015). The amount of sorbed antibiotic was calculated by using (eq. 1):

$$q_t = \frac{(C_0 - C_t)V}{m} \quad (1)$$

where q_t (mg g^{-1}) is the amount of adsorbed antibiotic at time *t*, C_0 and C_t are the antibiotic concentration in solution (mg L^{-1}) at t = 0 and t = *t*, *V* is the volume (L) of the antibiotic solution and *m* is the weight (g) of the sorbent. All experiments were carried out in triplicate. The mean values are reported and the error range was inferior to 5 %.

The kinetics parameters of the sorption reactions were determined using Lagergren pseudo-first and pseudo-second order models (Ho 2006). The first model (eq. 2)

$$\frac{dq_t}{dt} = k_1(q_{e,1} - q_t) \quad (2)$$

provides $q_{e,1}$ the calculated amount of adsorbed antibiotic at equilibrium (mg g^{-1}) and k_1 the first order kinetic constant (min^{-1}). The second model (eq. 3)

$$\frac{dq_t}{dt} = k_2(q_{e,2} - q_t)^2 \quad (3)$$

gives $q_{e,2}$ the calculated amount of adsorbed antibiotic at equilibrium (mg g^{-1}) and k_2 the second order kinetic constant (g $mg^{-1}min^{-1}$).

Experimental data obtained through sorption isotherms were analyzed using the Langmuir and Freundlich models (Mittal et al. 2007). Langmuir equation (eq. 4)

$$q_e = q_{e,max} \frac{\beta C_e}{1+\beta C_e} \quad (4)$$

allows the calculation of $q_{e,max}$ the maximum amount of adsorbed antibiotic at equilibrium (mg g^{-1}), and β is the Langmuir constant ($L.mg^{-1}$) related to the adsorption energy. The Freundlich equation model (eq. 5)

$$q_e = K_f C_e^{(1/n)} \quad (5)$$

leads to the determination of K_f the Freundlich constant correlated to the maximum adsorption capacity and n the adsorption intensity, respectively.

Results and discussion

The thermal degradation of the raw OST powder under air was studied by TGA. As shown in **Fig. 2**, after desorption of weakly bound water, a progressive loss of weight attributed to organic matter decomposition, was observed between 200°C and 700°C, accounting for ca. 4 w% of the initial material. The specific surface area of the OST 100, OST 550 and OST950 samples is also reported on **Fig. 2.** These values are very similar for the first two samples (ca. 25 $m^2.g^{-1}$), confirming that a fraction of the organic matter has been degraded without a strong impact on the mineral particle at 550°C. In contrast, the S_{BET} dropped down below 5 $m^2.g^{-1}$ for OST950, suggesting that after full degradation of the organic matter, mineral grain coarsening has occurred.

XRD analyses of the OST100 powder mainly shows the diffraction peaks of quartz (**Fig. 3**). Additional minor peaks at 2θ = 29.2°, 34.8° and 61.8° may correspond to calcite as well as alumina- and iron-rich phases, according to elemental analysis, but they cannot be unambiguously attributed. The XRD diffractogram of OST550 was very similar to that of OST100 except that these additional peaks were of relative lower intensity. Finally, for OST950, these two phases are no longer clearly identified but two additional peaks at 2θ = 30.0° and 33.3° are present that may correspond to the more intense diffraction peaks of the magnetite (Fe_3O_4) and hematite (Fe_2O_3) structures, respectively.

The OST powders were also studied by solid state NMR. The ^{29}Si spectra recorded by HPDEC-MAS showed for all samples a main resonance at 108 ppm, corresponding to fully condensed Q_4 (*i.e.* $Si(OSi)_4$) silicon species, as expected for quartz (**Fig. 4a**). A weak broad signal is found at higher chemical shifts (*ca.* - 95 ppm)

whose relative intensity decreases with heating temperature. This signal can be attributed to aluminosilicate species $Si(OSi)(OAl)_2(OH)$ ($Q_3(2Al)$), $Si(OAl)_3(OH)$ ($Q_3(3Al)$) or $Si(OSi)(OAl)_3$ ($Q_4(3Al)$) as typically found in phyllosilicates and zeolites (Engelhardt and Michel 1987). It is worth noticing that no signal corresponding to Q_3 (i.e. $Si(OSi)_3(OH)$) species could be observed at *ca*. -100 ppm, suggesting the absence of amorphous silica. In parallel, the ^1H NMR spectrum of the OST100 sample consists of a broad signal accompanied with multiple spinning side bands (**Fig. 4b**). This comb-like spectrum feature is typically obtained at this magnetic field for a sample containing a non-negligible amount of paramagnetic species. Sample heating led to a decrease of the intensity of the signal with annealing temperature so that only a very enlarged and noisy probe signal was obtained for the 950° heat-treated specimen (not shown).

^{27}Al MQ-MAS experiments allowed for a more detailed exploration of aluminium environment (**Fig. 5**). For OST100, the 2D map recorded with a long recycle delay (100 ms) allows for the detection of both Al(IV) and Al(VI), between 80 and 40 ppm and 0 and -40 ppm, respectively (**Fig. 5a**). With a shorter recycle delay (1 ms), the correlation peak area of Al(IV) species rises in intensity, suggesting that these species are relaxing faster than Al(VI) species (**Fig. 5b**). In parallel, the signals of Al(IV) species with high quadrupolar constants are broadened (as shown in the dashed rectangles). This strongly suggests the presence of paramagnetic species in the close proximity of the Al sites. For OST950, the Al(VI) species are no longer visible. The correlation peak area for Al(IV) species is unusually broadened, especially at short recycle delay (**Fig. 5c**). Noticeably, XRD studies have shown that at this temperature several diffraction peaks of low intensity that were attributed to Al-rich and Fe-rich phases have disappeared while iron oxide phases have grown. Therefore, it is possible to suggest that the thermal treatment leads to the formation of Al-substituted iron oxides. This is in agreement with the literature showing that magnetite and goethite can incorporate Al^{3+} ions that preferentially occupy tetrahedral sites of the iron oxide structure (Schwertmann and Murad 1990).

Kinetics investigations were carried out to measure the rate of sorption of the antibiotics under various experimental conditions and to determine the time required to reach equilibrium of the adsorption process (**Fig. 6**). The resulting data suggest that OTC and CIP are readily adsorbed onto OST surfaces within the first ten minutes, whereas the OFL required more than 5 hours to reach equilibrium. The thermal treatment of the oil shale had a minor impact on the sorption of OTC and CIP but greatly slowed down that of OFL. The pseudo-first order and the pseudo-second-order kinetics models were evaluated to reproduce the sorption data. The corresponding kinetics parameters are given in **Table 1**. The pseudo-second order model was the most accurate for the three antibiotics independently of the thermal treatment of the sorbents, except for OFL for OST100 and

OST500. The kinetics constants vary in the order k_2(OTC) >> k_2(CIP) > k_2(OFL) in all conditions. As pointed out by Al-Qodah et al., due to the large size of the antibiotics, the sorption kinetics may be strongly affected by mass transfer limitations, either external (from the solution to the sorbent surface) or internal (within the OST porosity) (Al-Qodah et al. 2003b). However, one should note that the fastest kinetics are obtained for the largest molecule, *i.e*. OTC, suggesting that these diffusional effects do not play a major role when the different antibiotics are compared.

The effect of the amount of powder on the antibiotic sorption was then studied for OST100 (**Fig. 7).** A substantial increase in the amount of retained molecules was observed for oil shale doses up to 2 g L^{-1}. Above this value, surface saturation of the sample was reached for OTC whereas the amount of immobilized OFL and CIP continued to increase, although at a much lower rate. The thermal treatment of the powders did not significantly modify these trends. On this basis, a 2 g L^{-1} dose of the OST powder was selected for the rest of our study.

The retention capacity of raw oil shale OST100 and the heat-treated OST550 and OST950 powders was then studied by performing sorption isotherms for initial antibiotic concentrations ranging from 5 mg L^{-1} to 100 mg L^{-1} over 24 h (**Fig. 8**). For CIP and OFL, OST saturation was reached in this concentration range and experimental maximum sorption efficiency q_{max} varied from 37 mg g^{-1} to 1 mg g^{-1}. They were larger for CIP compared to OFL for a given sorbent and systematically decreased with heating temperature. For OTC, a similar decrease of q_{max} with sample heating was observed, from 40 mg g^{-1} for OST100 to 26 mg.g^{-1} for OST950, but the sorption isotherms did not reach a plateau.

Langmuir and Freundlich isotherm models were tested to simulate the experimental data for the adsorption of the three antibiotics on the three OST powders. The parameters extracted from these analyses are gathered in **Table 2**. The most reliable fits (i.e. larger R^2 values) were obtained with the Langmuir model. The calculated maximum sorption efficiency $q_{e,max}$ were in the order OTC > > CIP > OFL for all sorbents. For CIP and OTC, $q_{e,max}$ decreased by 10-20 % from OST100 to OST550 and then by ca. 40 % for OST950. In contrast, for OFL, the first heating step decreases its sorption by ca. 50 % and the second one by more than 85 %. No clear trend in the evolution of the Langmuir parameter with antibiotic nature or OST treatment could be identified.

To analyze these data, it is first important to consider the relative charge of the powders and antibiotics. The isoelectric point (IEP) of quartz was reported to vary between 1.5 and 3, so that it is negatively-charged in the conditions of these experiments (Komulski 2016; Parks 1965). It is well-admitted that the heat-treatment of metal oxide phases favor the condensation of M-OH groups to form more M-O-M bonds, increasing the basicity

of the surface so that an increase in the IEP of OST with temperature treatment is expected (Zhuravlev 2000). Noticeably, the content of the organic matter found is oil shale can range from acidic macromolecules from plant or algal origin to large polyphenolic structures depending on the extent of the diagenesis process (Siskin and Katritzky 1991). They can therefore contribute to the acid-base properties of the OST100 powders and their removal upon heating should also impact on the material sorption properties.

Considering antibiotics, CIP and OFL have a very similar profile considering the effect of pH on their charge (**Fig. 9a**). They both have an aromatic carboxylic acid group (1 and 1' on **Fig. 1**) with a pKa of *ca*. 6 and amine groups belonging to a piperazinyl ring (2 and 2') with pKa of ca. 8.5. Therefore, they are mainly positively charged up to pH 7.5. For OTC, the tricarbonyl methane part (3) has a pKa of 3.3, the dimethylammonium group (4) of 7.3 and the phenolic diketone group (5) of 9.1. Therefore OTC charge ranges from 0 to -2 in the 5-10 pH range.

Altogether, from an electrostatic point of view, the antibiotic sorption on OST surface at pH 5 is strongly favoured for OFL and CIP whereas a lower affinity is expected for OTC. However, this is in apparent contradiction with the higher sorption efficiency obtained for OTC and lower sorption of OFL. Rather, the observed trend in the sorption efficiency of the three antibiotics in good agreement with their hydrophobic character that can be evaluated by their octanol-water partition coefficients XlogP3 value (Cheng et al. 2007), ranging from -0.4 for OFL to -1.6 for OTC (**Fig. 1**). To clarify this point, the influence of pH on antibiotic retention by OST 100 was studied. As shown in **Figure 9b**, the amount of sorbed OFL decreases sharply with increasing pH, in agreement with the parallel shift of its charge from positive to negative, leading to unfavourable repulsive electrostatic interactions. The amount of retained CIP also decreases at higher pH but more moderately than for OFL. This supports our previous assumption that hydrophobic interactions have an important contribution in the sorption of CIP on OST surface. This contribution becomes prevalent for OTC whose sorption does not vary significantly with increasing pH despite the fact that its charge turns negative.

Considering the effect of oil shale thermal treatment, it must be reminded that the first heating step from 100°C to 550°C does not significantly modify the mineral surface chemistry, nor the powder porous structure. Therefore the observed decrease in sorption capacity can be mainly attributed to the partial removal of the organic matter. This is in agreement with the literature showing that OTC sorption is favoured in soils containing high amount of organic matter (Kong et al. 2012). Heating further to 950°C sample, the specific surface area decreases by one order of magnitude, and the surface becomes more hydrophobic due to the condensation of Si-OH, Al-OH and even Fe-OH groups (Zhuravlev 2000). It can therefore be proposed that, for the more

hydrophobic OTC and CIP molecules, the decrease in available surface is partly balanced by the increase in surface hydrophobicity, resulting in moderate decrease in kinetics rate and maximum sorption capacity. In contrast, for the more hydrophilic OFL, such a balance does not exist, resulting in a very important decrease of these two parameters.

The sorption process was well reproduced using a Langmuir model, suggesting that the antibiotics form a homogeneous single layer on the OST surface. However, the kinetics data were best fitted using a pseudo-second order model in which the sorption rate depends on the square of the antibiotic concentration. This suggests that antibiotic molecules tend to form dimers in the aqueous solution before adsorption. This assumption is supported by previous theoretical calculations showing that several hydrophobic drugs have a strong tendency to form mixed-charge dimers associating neutral and charged forms of the molecules (Avdeev 2014). This should be particularly true for OFL and CIP for which zwitterionic and anionic form coexist over a wide range of pH.

Finally, it must be pointed out that the sorption efficiency determined in this work for CIP and OFL are in an intermediate range of reported values for other mineral sorbents, activated carbons and biomass extracts (El-Shafey 2012; Liu et al. 2013; Wang et al. 2014; Zhang et al. 2012). For OTC, the OST100 sorption efficiency (*ca*. 50 mg g^{-1}) is larger than those reported for biochar (*ca*. 5 mg g^{-1}) (Jia et al. 2013), clays (*ca*. 10 mg g^{-1}) (Bansal 2013) and iron oxide (*ca*. 20 mg g^{-1}) (Figueroa and MacKay 2005). Our data suggest that these higher retention rates can be attributed to the fact that this antibiotic and the mineral surface share a common hydrophobic character.

Conclusion

Oil shale raw materials have so far been scarcely studied outside the field of fuel production. Here we show that they can exhibit relatively high affinity for some pharmaceutical products, due to the coexistence of organic matter and mineral phases, and may therefore contribute to their accumulation in soils. Moreover, these materials preserve good sorption properties after high temperature thermal treatment, suggesting that they can be used as cheap sorbents for environmental cleaning.

Acknowledgments

The authors thank the CNRS (France) and CNRST (Morocco) for funding this research through the APATENV project of the PICS program.

References

Aboulkas A, El Harti K (2009) Effects of acid treatments on Moroccan Tarfaya oil shale and pyrolysis of oil shale and their kerogen. J Fuel Chem Technol 37:659-667.

Al-Qodah Z (2000) Adsorption of dyes using shale oil ash. Water Res 34:4295-4303.

Al-Qodah Z, Lafi W (2003) Adsorption of reactive dyes using shale oil ash in fixed beds, Water Supply 52:189-198.

Al-Qodah Z, Shawaqfehb AT, Lafi WK (2007a) Adsorption of pesticides from aqueous solutions using oil shale ash. Desalination 208:294-301.

Al-Qodah Z, Shawaqfeh AT, Lafi WK (2007b) Two-resistance mass transfer model for the adsorption of the pesticide deltamethrin using acid treated oil shale ash. Adsorption 13:73-82.

Avdeef A (2014) Anomalous solubility behavior of several acidic drugs. ADMET & DMPK 2:33-42.

Babel S, Kurniawan TA (2003) Low-cost adsorbents for heavy metals uptake from contaminated water: A review. J Hazard Mater B97:219-243

Bansal OP (2013) Sorption of tetracycline, oxytetracycline, and chlortetracycline in illite and kaolinite suspensions. ISRN Environ Chem 2013 Article ID 694681.

Bernard S, Horsfield B, Schulz HM, Schreiber A, Wirth R, Anh Vu TT, Perssen F, Könitzer S, Volk H, Sherwood N, Fuentes D (2010) Multi-scale detection of organic and inorganic signatures provides insights into gas shale properties and evolution, Chem Erde S3:119-133.

Bouyarmane H, El Hanbali I, El Karbane M, Rami A, Saoiabi A, Saoiabi S, Masse S, Coradin T, Laghzizil A (2015) Parameters influencing ciprofloxacin, ofloxacin, amoxicillin and sulfamethoxazole retention by natural and converted calcium phosphates. J Hazard Mater 291:38-44.

Bruan V, Halim M, Ziyad M, Largeau C, Amblès A (2001) Characterization of the Moroccan Timahdit (X-layer) oil shale kerogen using pyrolysis and thermally assisted hydrolysis and methylation. J Anal Appl Pyrol 61:165-179.

Carrasquillo AJ, Bruland GL, Mackay AA, Vasudevan D (2008) Sorption of ciprofloxacin and oxytetracycline zwitterions to soils and soil materials: influence of compound structure. Environ Sci Technol 42:634-7642.

Cheng T, Zhao Y, Li X, Lin F, Yong X, Zhang X, Li Y, Wang R, Lai L (2007) Computation of octanol-water partition coefficients by guiding and additive model with knowledge. J Chem Inf Model 47:2140-2148.

El-Shafey EI, Al-Lawati H, Al-Sumri AS (2012) Ciprofloxacin adsorption from aqueous solution onto chemically prepared carbon from date palm leaflets. J Environ Sci 24:1579–1586.

Engelhardt G, Michel D (1987) High-Resolution Solid-State NMR of silicates and zeolites. John Wiley & Sons Ltd. (New York).

Fernandes Machado NRC, Miotto DMM (2005) Synthesis of Na–A and –X zeolites from oil shale ash. Fuel 84:2289–2294.

Figueroa RA, Mackay AA (2005) Sorption of oxytetracycline to iron oxides and iron oxide-rich soils. Environ Sci Technol 39 :6664-6671.

Golet EM, Xifra I, Siegrist H, Alder AC, Giger W (2003) Environmental exposure assessment of fluoroquinolone antibacterial agents from sewage to soil. Environ Sci Technol 37: 3243-3249.

Gouza A, Saoiabi S, Masse S, Laghzizil A, Saoiabi A (2014) Development and characterization of oil shale minerals for ciprofloxacin remediation. J Chem Pharm Res 6:316-324.

Ho YS (2006) Review of second-order models for adsorption systems. J Hazard Mater 136:681-689.

Holditch SA (2013) Unconventional oil and gas resource development – Let's do it right. J Unconventional Oil Gas Resources 1-2:2-8.

Ichcho S, Khouya E, Fakhi S, Ezzine M, Hannache H, Pallier R, Naslain R (2005) Influence of the experimental conditions on porosity and structure of adsorbents elaborated from Moroccan oil shale of Timahdit by chemical activation. J Hazard Mater 118:45-51.

Irha N (2000) Sorption of pyrene from water by oil shale ash and mineral particles. Toxicol Environ Chem 74:105-110.

Jia M, Wang F, Bian Y, Jin X, Song Y, Kengara FO (2013) Effects of pH and metal ions on oxytetracycline sorption to maize-straw-derived biochar. Bioresource Technol 136:87-93.

Kagle J, Porter AW, Murdoch RW, Rivera-Cancel G, Hay AG (2009) Biodegradation of pharmaceutical and personal care products. Adv Appl Microbiol 67:65-108.

Komulski M (2016) Isoelectric points and points of zero charge of metal (hydr)oxides: 50 years after Parks' review. Adv Colloid Interface Sci 238:1-61.

Kong W, Li C, Dohli JM, Li S, He J, Qiao M (2012) Characteristics of oxytetracycline sorption and potential bioavailability in soils with various physical–chemical properties. Chemosphere 87:542-548.

Kümmerer K (2009a) Antibiotics in the aquatic environment -a review-Part I. Chemosphere 75:417-434.

Kummerer K (2009b) Antibiotics in the aquatic environment-a review-Part II. Chemosphere 75: 435-441.

Liu Z, Sun P, Pavlostathis SG, Zhou X, Zhan Y (2013) Adsorption, inhibition, and biotransformation of ciprofloxacin under aerobic conditions. Bioresource Technol 144:644-651.

Mittal A, Kurup L, Mittal J (2007) Freundlich and Langmuir adsorption isotherms and kinetics for the removal of Tatrazine from aqueous solutions using hen feathers. J Hazard Mater 146:243-248.

Parks GA (1965) The isoelectric points of solid oxides, solid hydroxides, and aqueous hydroxo complex systems. Chem Rev 65:177-198.

Ross DJK, Bustin RM (2009) The importance of shale composition and pore structure upon gas storage potential of shale gas reservoirs. Marine Petroleum Geol 26:916-927.

Shawabkeh R, Al-Harahsheh A, Al-Otoom A (2004) Copper and zinc sorption by treated oil shale ash. Sep Purif Technol 40:251-257.

Schwertmann U, Muran E (1990) The influence of aluminium on iron oxides: XIV. Al-substituted magnetite synthesized at ambient temperature. Clays Clay Miner 38:196-202.

Siskin M, Katritzky AR (1991) Reactivity of organic compounds in hot water: geochemical and technological implications. Science 254:231-237.

Tütem E, Apak R, Üna CF (1998) Adsorptive removal of chlorophenols from water by bituminous shale. Water Res. 32:2315-2324.

Vasudevan D, Bruland GL, Torrance BS, Upchurch VG, Mackay AA (2009) pH-dependent ciprofloxacin sorption to soils: interaction mechanisms and soil factors influencing sorption. Geoderma 151:68-76.

Wang DM, Xu YM, He DM, Guan J, Zhang OM (2009) Investigation of mineral composition of oil shale. Asia-Pac J Chem Eng 4:691–697.

Wang Q, Zhang J, Zheng Y, Wang A (2014) Adsorption and release of ofloxacin from acid- and heat-treated halloysite. Colloids Surf B 113:51-58.

Zhang CL, Zhao F, Wang Y (2012) Thermodynamic and kinetic parameters of ofloxacin adsorption from aqueous solution onto modified coal fly ash. Russian J Phys Chem A 86:653-657.

Zhu S, Bell PRF, Greenfield PF (1988) Adsorption of pyridine onto spent Rundle oil shale in dilute aqueous solution. Water Res 22:1331-1337.

Zhuravlev LT (2000) The chemistry of amorphous silica. Zhuravlev model. Colloids Surf A 173:1-38.

Table 1. Kinetic rate constants (k_i) and adsorption capacities ($q_{e,i}$) obtained by using pseudo-first order and pseudo-second order models to CIP , OTC and OFL antibiotics on the oil shale sorbents. R^2 indicate the correlation coefficients for the linear fits.

		Pseudo first order model			Pseudo second order model		
		k_1 (min^{-1})	$q_{e,1}$ (mg g^{-1})	R^2	k_2 (g mg^{-1}.min^{-1})	$q_{e,2}$ (mg g^{-1})	R^2
OST100	OTC	0.102	1.12	0.9767	0.0388	8.44	0.9995
	OFL	0.007	7.12	0.9858	0.0003	8.56	0.9464
	CIP	0.012	2.92	0.9167	0.0150	9.45	0.9993
OST550	OTC	0.133	1.88	0.9644	0.0299	9.25	0.9997
	OFL	0.009	6.13	0.9904	0.0007	5.68	0.9650
	CIP	0.012	3.64	0.9958	0.0090	9.46	0.9995
OST950	OTC	0.013	0.62	0.7167	0.0958	7.45	0.9999
	OFL	0.006	1.14	0.9779	0.0020	1.31	0.9905
	CIP	0.003	1.28	0.9732	0.0020	3.93	0.9928

Table 2. Langmuir and Freundlich constants for antibiotics sorption on the OST100, OST550 and OST950 adsorbents.

		Exp.	Langmuir			Freundlich		
		q_{max} (mg g^{-1})	$q_{e,max}$ (mg g^{-1})	β (L mg^{-1})	R^2	log K_f	1/n	R^2
OST100	CIP	37.7	43.4	0.034	0.9853	0.66	0.54	0.9353
	OFL	13.5	15.4	0.099	0.9897	0.43	0.42	0.7635
	OTC	>41	69.8	0.060	0.9667	0.84	0.04	0.9039
OST550	CIP	24.9	27.4	0.048	0.9944	0.75	0.33	0.9244
	OFL	6.6	8.2	0.056	0.9894	0.24	0.60	0.9126
	OTC	>35	61.4	0.040	0.9848	0.80	0.03	0.9041
OST950	CIP	15.3	18.2	1.020	0.9413	0.05	0.58	0.9413
	OFL	0.98	1.53	0.020	0.9985	-1.26	0.67	0.9365
	OTC	>26	35.3	0.060	0.9975	0.84	0.01	0.8284

Figure Captions

Fig.1 Chemical formula, molecular weights (*MW*), main *pKa* values and calculated octanol-water partition coefficients (*XlogP3*) of antibiotics used in this study

Fig. 2 Thermogravimetric analysis of the oil shale powders and the specific surface area S_{BET} of the powders at after thermal treatment at 100°C, 550 °C and 950°C (from Gouza et al. 2014).

Fig. 3 XRD diffractograms of OST100, OST 550 and OST950. Q = quartz; A = Alumina; I = hydrated iron phase; M= magnetite; H = hematite; C = calcite

Fig. 4 (a) ^{29}Si HPDec MAS NMR spectra of (blue) OST100, (green) OST550 and (purple) OST950 samples; (b) ^{1}H MAS NMR spectra of OST 100. ***** spinning side bands equidistant of 5 kHz at both sides from the central signal.

Fig. 5 ^{27}Al 3Q-MAS NMR spectra of (a) OST 100 – recycle delay 100 ms; number of scans 14,000; (b) OST100 – recycle delay 1 ms; number of scans 57,000; (c) OST950 – recycle delay 1 ms; number of scans 57,000. CS = chemical shift; QSI = quadripolar-induced shift. The dashed rectangles correspond to the same spectral area.

Fig. 6 Evolution of the amount of sorbed antibiotic (q_t) with contact time *t* for (a) oxytetracycline OTC (b) ofloxacine OFL and (c) ciprofloxacin CIP on the oil shale samples. Plain lines (—) correspond to the simulation of experimental data with the pseudo-second order model**.**

Fig. 7 Evolution of sorbed antibiotic content (q_e) for (a) OCT and (b) OFL and CIP as a function of the OST powder dose. Plain lines are provided for eye guidance only.

Fig. 8 Variation of sorbed antibiotic content (q_e) with antibiotic concentration at equilibrium (C_e) after 24 h of contact with the OST powders for (a) oxytetracycline OTC (b) ofloxacine OFL and (c) ciprofloxacin CIP. Plain lines (—) correspond to the curves obtained by fitting the data with the Langmuir equation**.**

Fig. 9 (a) Calculated average charge per molecule for the three antibiotics and (b) experimental amount of retained antibiotic (q_e) on OST100 (C_0 = 30 mg.L^{-1})) as a function of pH.

Fig. 1

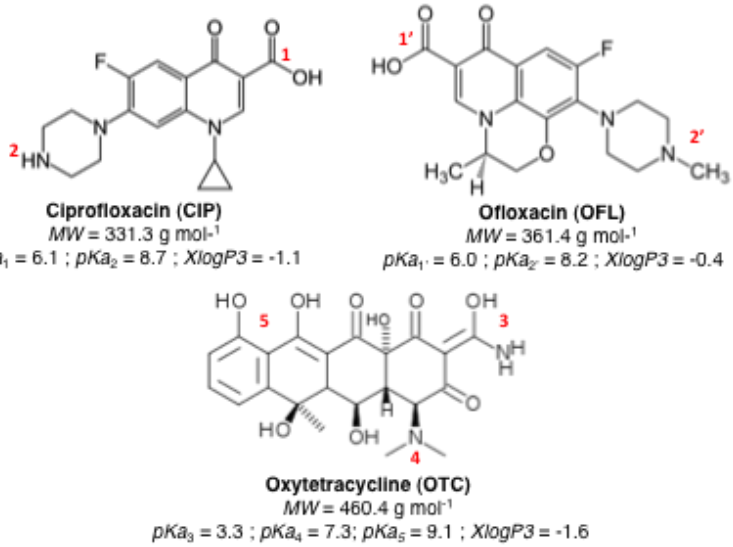
F
O
O
1
OH
2
HN
N
N
Ciprofloxacin (CIP)
MW = 331.3 g mol-1
pKa1 = 6.1 ; pKa2 = 8.7 ; XlogP3 = -1.1
1'
HO
O
O
F
N
N
2'
H3C
O
N
CH3
H
Ofloxacin (OFL)
MW = 361.4 g mol-1
pKa1' = 6.0 ; pKa2' = 8.2 ; XlogP3 = -0.4
HO
5
OH
O
HO
O
OH
3
NH
H
O
HO
OH
N
4
Oxytetracycline (OTC)
MW = 460.4 g mol-1
pKa3 = 3.3 ; pKa4 = 7.3; pKa5 = 9.1 ; XlogP3 = -1.6

Fig. 2

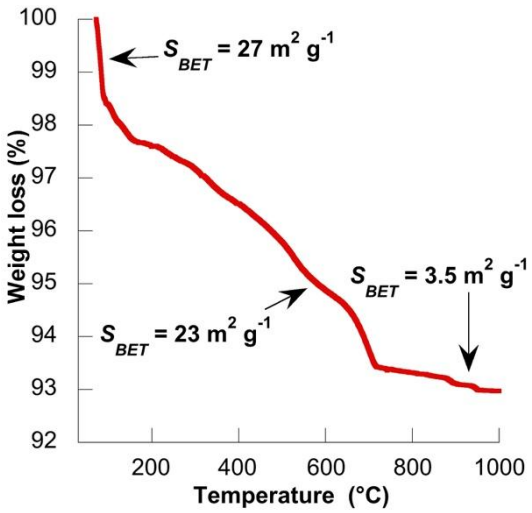
100
99
98
97
96
95
94
93
92
Weight loss (%)
S_{BET} = 27 m^2 g^{-1}
S_{BET} = 23 m^2 g^{-1}
S_{BET} = 3.5 m^2 g^{-1}
200
400
600
800
1000
Temperature (°C)

Fig. 3

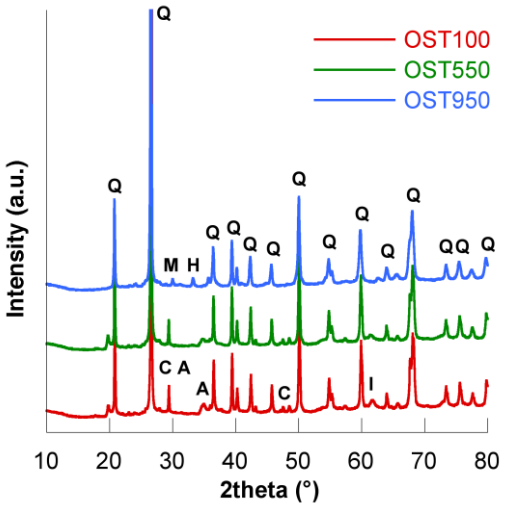
OST100
OST550
OST950
Intensity (a.u.)
2theta (°)
10
20
30
40
50
60
70
80
Q
M H
C A
A
C
I

Fig. 4

(a) ^{29}Si HPDec MAS NMR

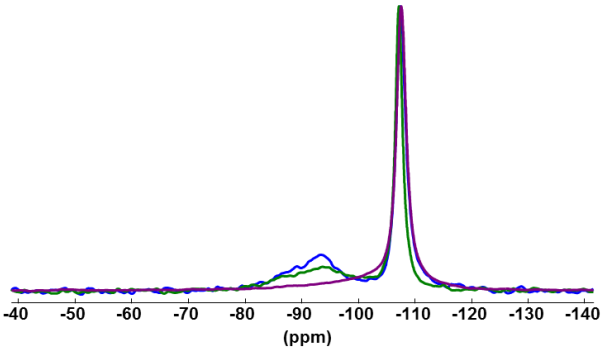

(b) ^{1}H MAS NMR

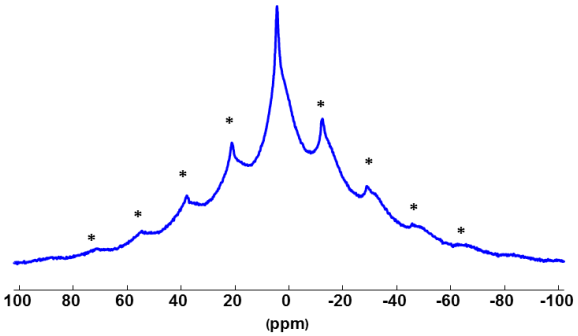

Fig. 5

(a)

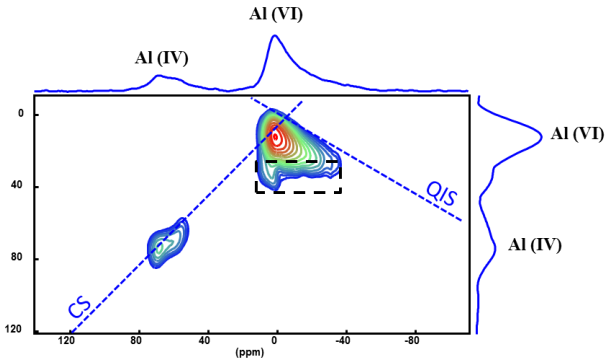
Al (VI)
Al (IV)
Al (VI)
Al (IV)
QIS
CS
0
40
80
120
120
80
40
0
-40
-80
(ppm)

(b)

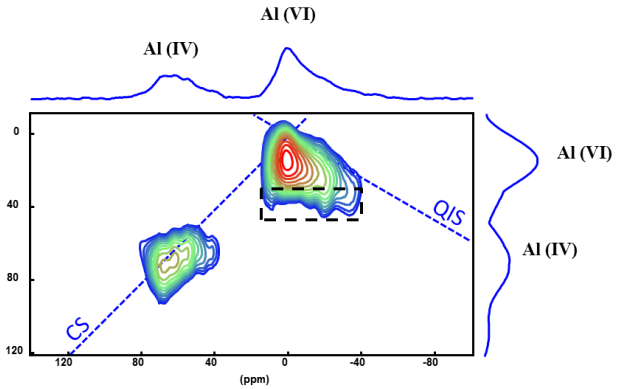
Al (VI)
Al (IV)
Al (VI)
Al (IV)
QIS
CS
0
40
80
120
120
80
40
0
-40
-80
(ppm)

(c)

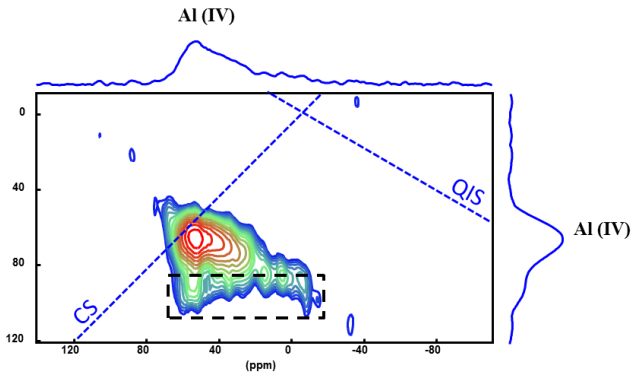
Al (IV)
Al (IV)
QIS
CS
0
40
80
120
120
80
40
0
-40
-80
(ppm)

Fig. 6

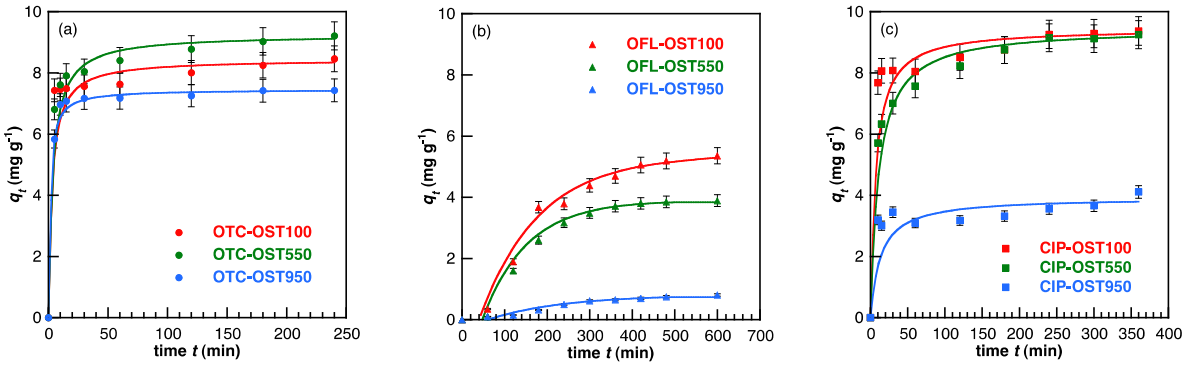
(a)
OTC-OST100
OTC-OST550
OTC-OST950
q_t (mg g^{-1})
time t (min)
(b)
OFL-OST100
OFL-OST550
OFL-OST950
q_t (mg g^{-1})
time t (min)
(c)
CIP-OST100
CIP-OST550
CIP-OST950
q_t (mg g^{-1})
time t (min)

Fig. 7

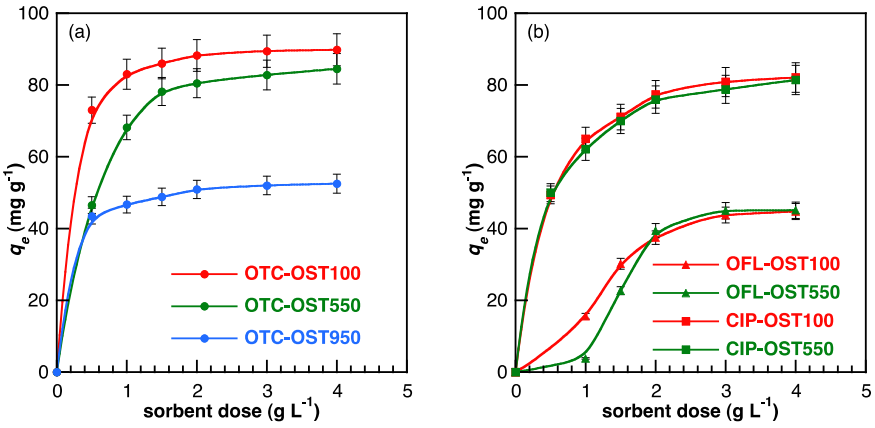
(a)
100
80
60
40
20
0
0
1
2
3
4
5
q_e (mg g^{-1})
sorbent dose (g L^{-1})
OTC-OST100
OTC-OST550
OTC-OST950
(b)
OFL-OST100
OFL-OST550
CIP-OST100
CIP-OST550

Fig. 8

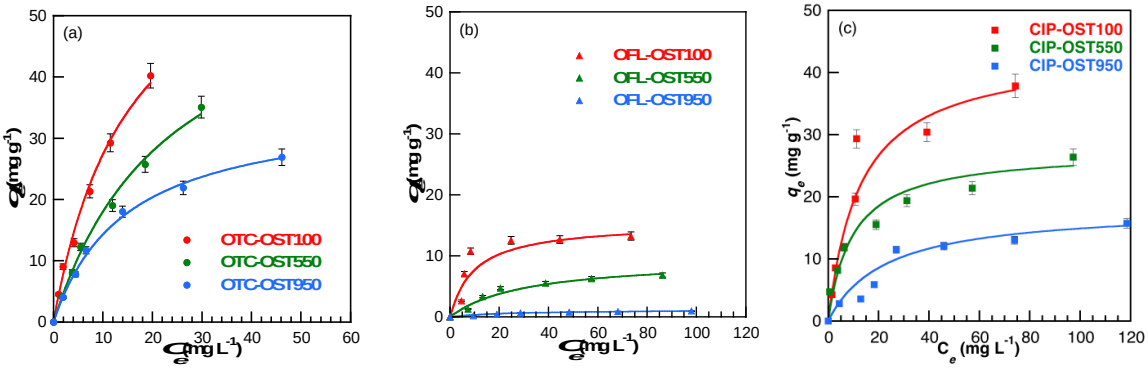
(a)
OTC-OST100
OTC-OST550
OTC-OST950
(b)
OFL-OST100
OFL-OST550
OFL-OST950
(c)
CIP-OST100
CIP-OST550
CIP-OST950

Fig. 9

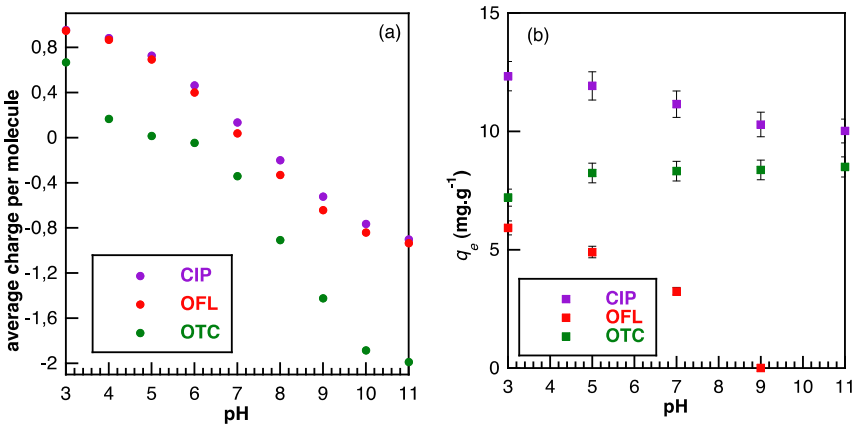
(a)
average charge per molecule
0,8
0,4
0
-0,4
-0,8
-1,2
-1,6
-2
3
4
5
6
7
8
9
10
11
pH
CIP
OFL
OTC
(b)
q_e (mg.g^{-1})
15
10
5
0
3
4
5
6
7
8
9
10
11
pH
CIP
OFL
OTC